VIP Lithium-Ion Batteries Very Important Paper

DOI: 10.1002/anie.201404197

In Situ Quantification and Visualization of Lithium Transport with Neutrons**

Danny X. Liu, Jinghui Wang, Ke Pan, Jie Qiu, Marcello Canova, Lei R. Cao, and Anne C. Co**

Abstract: *A real-time quantification of Li transport using a nondestructive neutron method to measure the Li distribution upon charge and discharge in a Li-ion cell is reported. By using in situ neutron depth profiling (NDP), we probed the onset of lithiation in a high-capacity Sn anode and visualized the enrichment of Li atoms on the surface followed by their propagation into the bulk. The delithiation process shows the removal of Li near the surface, which leads to a decreased coulombic efficiency, likely because of trapped Li within the intermetallic material. The developed in situ NDP provides exceptional sensitivity in the temporal and spatial measurement of Li transport within the battery material. This diagnostic tool opens up possibilities to understand rates of Li transport and their distribution to guide materials development for efficient storage mechanisms. Our observations provide important mechanistic insights for the design of advanced battery materials.*

Lithium-ion batteries (LIBs) are the most promising technology amongst the rechargeable energy storage systems, and their high gravimetric and volumetric energy density have led to them being widely used in a broad range of industrial and consumer applications. Although still dominating portable electronics, LIBs are now being considered for the storage and distribution of renewable energy sources and in the automotive industry, for powering electric and plug-in hybrid vehicles. The increasing demand for LIBs has stimulated the development of advanced materials, diagnostic tools, and battery models that could lead to better performance in terms of storage capacity, kinetics, and long-term cyclability.

A nondestructive method for the real-time visualization and quantification of Li ions could be a powerful tool for understanding Li storage properties and guide the development of durable, cyclable, and efficient storage materials, especially as Li insertion or diffusion through solids is often the rate-limiting step in battery processes.[1] A direct measurement of Li distribution within a material in real time can provide valuable information for modeling Li transport at the fundamental and systems level.

In situ X-ray diffraction (XRD), Mössbauer spectroscopy, nuclear magnetic resonance, transmission electron microscopy, scanning probe microscopy (AFM, STM), and synchrotron X-ray tomography[2] have been used to quantify crystal-structure evolution and visualize the expansion/contraction of electrode materials during lithiation and delithiation processes, with each having their own advantages and limitations. An in situ neutron technique such as neutron depth profiling (NDP),[3] while relatively new for applications in battery materials research, could be powerful because of its high sensitivity to certain light elements (e.g. ^{6}Li, ^{10}B, ^{14}N, ^{7}Be). This selective nature of neutrons results in spectra that allow the direct tracking and counting of Li atoms without resorting to inferring Li transport phenomena from indirect observations.

A real-time quantification of Li transport using a nondestructive neutron method to measure the Li distribution upon charge and discharge is reported here. As a neutral particle that has a selective interaction probability with different isotopes, a neutron is ideal for probing Li atoms deep inside the battery. We have developed an in situ technique based on NDP to provide temporal and spatial measurement of Li within a material and to visualize its transposition during dynamic charging and discharging. Our experimental design also allows for measurements in low vapor pressure "wet" electrolyte inside the evacuated NDP chamber, which opens up possibilities for probing a variety of energy storage materials, ultimately providing information to guide materials development for efficient energy storage. Herein, we explored the onset of lithiation in a model Sn electrode by using in situ NDP and visualized the enrichment of Li atoms on the surface while monitoring the propagation of Li into the bulk. NDP provides valuable mechanistic insights for evaluating the transport of light elements.

NDP is a quantitative analytical technique for measuring elements that exhibit a high probability of absorbing neutrons as a function of depth (Figure 1). ^{6}Li absorbs neutrons (with a probability of 940 barns for neutron energy at 25 meV and

[*] D. X. Liu, Prof. A. C. Co
Department of Chemistry and Biochemistry
The Ohio State University
100 West 18th Avenue, Columbus, OH 43210 (USA)
E-mail: co@chemistry.ohio-state.edu
J. Wang, Dr. J. Qiu, Prof. L. R. Cao
Nuclear Engineering Program, The Ohio State University
201 West 19th Avenue, Columbus, OH 43210 (USA)
E-mail: cao.152@osu.edu
K. Pan, Prof. M. Canova
Department of Mechanical and Aerospace Engineering
The Ohio State University
201 West 19th Avenue, Columbus, OH 43210 (USA)

[**] This work was supported by the Clean Energy Research Center-Clean Vehicle (CERC-CV) Consortium, the U.S. Department of Energy, the Department of Chemistry and Biochemistry, and the Institute for Materials Research at The Ohio State University. We would like to thank Dr. R. Gregory Downing from NIST for useful discussions and the use of the NDP facility at NCNR. We also thank the support from staff at The Ohio State University Nuclear Reactor Laboratory and the University of Maryland Outreach Program for travel support.

Supporting information for this article is available on the WWW under http://dx.doi.org/10.1002/anie.201404197.

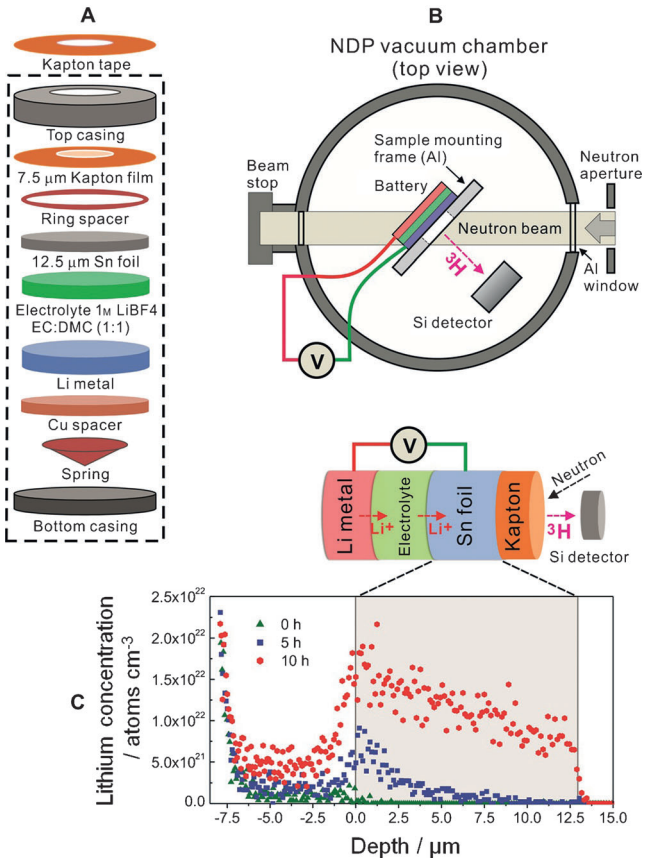

Figure 1. A) A schematic representation of the battery components. B) Illustration of the NDP chamber at NCNR. C) Three snapshots of the in situ NDP spectra showing Li transport during charging/discharging a battery. EC = ethylene carbonate, DMC = dimethyl carbonate.

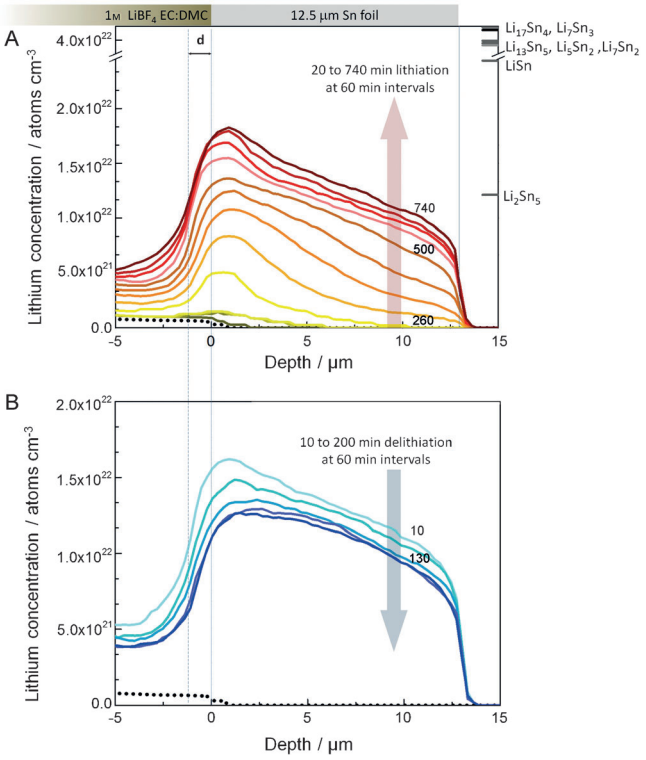

Figure 2. Lithium concentration profiles within a 12.5 μm Sn foil as a function of time. Dashed lines: before electrochemical lithiation. A) Lithiation spectra plotted every 60 min interval from 20 min to 740 min at 0.4 V versus Li/Li^+ (reaching ca. 200 $mAhr\,g^{-1}$). B) Delithiation spectra plotted every 60 min interval from 10 min to 200 min delithiation at 1.0 V versus Li/Li^+.

2116 barns at 5 meV) governed through the nuclear reaction shown in Equation (1).

$$n + {}^6\mathrm{Li} \rightarrow {}^4\mathrm{He} + {}^3\mathrm{H} + 4.8\,\mathrm{MeV} \quad (1)$$

The initial and final energies of both emitted alpha (^{4}He) and triton (^{3}H) particles are quantified and the corresponding Li depth profile can be directly determined from the atomic composition and density of the electrode material. Figure 2 shows Li transposition through a dense 12.5 μm Sn film and various components of an electrochemical cell, with a total traveling distance of approximately 20 μm.

Recently, efforts in the development of LIB electrode materials have focused on a class of elements that form stable intermetallic compounds with Li and provide Li storage capacities 3 to 10 times that of conventional graphite anodes.[4] Lithiation and delithiation of high energy density intermetallic electrode materials, such as LiSi, LiSn, LiGe, LiPb, LiSn, LiAg, and combinations thereof, are often accompanied by phase transitions and transformations that result in electrochemically driven amorphization[5] and large volume changes that influence cyclability. For example, in the case of Sn, the lithiation process transforms Sn through its thermodynamically stable phases of Li_2Sn_5, LiSn, Li_7Sn_3, Li_5Sn_2, $Li_{13}Sn_5$, Li_7Sn_2, and $Li_{17}Sn_4$ with increasing Li content, and has been observed to expand up to 300 % in volume at full charge, which results in mechanical deformation and fracture.[2b,c,e] Materials structures such as nanowires, 3D architectures, and inactive core/active shell systems allows the accommodation of changes induced by these transformations, thereby offering improved performance and lifetime.[6] However, the transport properties of lithium and its resulting distribution within the material are largely inferred by using ex situ and often invasive techniques.

The experimental study was performed by designing a sealed electrochemical cell (Figure 1) for keeping low vapor pressure "wet" electrolytes in a vacuum while allowing nuclear reaction products to pass through a thin Kapton film (ca. 7.5 μm) to the detector. An all-solid-state thin film battery has been previously reported to avoid any liquid components for NDP study.[7] Our design allows depth resolution that enables lithium transport properties to be elucidated as particles travel through a material with known atomic composition and densities. Additionally, this design allows quantification of changes in the Li concentration in the electrode directly without having to first obtain a background spectrum. The electrochemical cell consists of a uniform thin-layer metallic Sn foil (12.5 μm) to ensure a well-defined current distribution across the electrode during the lithiation and delithiation processes. The working electrode, a 300 μm

Li foil, serves as both the counter and reference electrode separated by a 25 μm Celgard immersed in a conventional carbonate electrolyte (1M $LiBF_4$ in EC:DMC), which mimics an operating battery. Lithiation potentials and the total charge passed were carefully selected to minimize mechanical fracture.

The distribution of Li in working batteries undergoing charge/discharge cycles reported herein was measured using the NDP facility at the National Institute of Standards and Technology's (NIST) Center for Neutron Research (NCNR), while the optimization of the electrochemical design and preliminary in situ testing were initially performed at The Ohio State University Research Reactor. Although neutrons will only interact with ^{6}Li, all the lithium concentrations reported herein account for the total Li content assuming a natural abundance of 7.5% for ^{6}Li. Lithium and boron standards were used to calibrate the channel number to energy, and the counts per channel to the Li concentration (see the Supporting Information). With the aid of a simulation code called "Stopping and Range of Ions in Matter" (SRIM), the energy loss of the triton particle to the different cell components was calculated and used for calibrating depth penetration. NDP spectra collected during charge and discharge cycles were recorded every 5 min during a potentiostatic hold at +0.4 V versus Li/Li^+ (lithiation) over a period of approximately 12 h, which amounts to approximately 200 mAhr g^{-1}. The 1σ relative counting uncertainty shown in Figure 1 C of about 3% is mainly due to the random nature of nuclear counting. Counting each spectrum for longer would give better counting statistics, however, at the price of worsening time resolution for the in situ NDP study. The dominant error in the NDP spectra stems from a systematic error used to calibrate depth. Herein, the density of a pure 12.5 μm Sn was used to calibrate the depth, while in reality the electrode composition changes as a function of charge and discharge, which could influence the stopping power of the materials for the charge particles. Taking into account the differences in the physical properties of lithiated Sn and the components in the electrochemical cell, an overall conservative estimate of about 10% uncertainty is assumed for the NDP spectra.

A real-time evolution of the Li profile during charge and discharge was determined (see Movie S1 in the Supporting Information). Figure 2 depicts snap shots of the Li distribution (smoothed using a running median filter) at 60 min intervals, tracking the Li distribution as a function of charge and discharge. The depth intervals (Figure 2) are generally classified as the electrolyte region (−5 to 0 μm), "near surface" region (0 to 1 μm), and the bulk Sn (>5 μm), where 0 um is assigned to the Sn electrode/electrolyte interface. Prior to lithiation (Figure 2 black dashed line), the Li signal in the electrolyte region (−5 to 0 μm) corresponds to $6.2(\pm0.6)\times10^{20}$ atom cm^{-3}, which is equivalent to the concentration of Li in 1M $LiBF_4$. Upon lithiation, it is evident that an enrichment of Li at the near surface region (up to 2 μm) of Sn is prevalent (0 to 260 min), which is followed by the diffusion of Li into the bulk. The surface concentration of Li reaches a steady state at $1.9(\pm0.3)\times10^{22}$ atoms cm^{-3} by 680 min (equivalent to ca. 200 mAhr g^{-1}).

An asymmetric Li peak centered at about 0.6 μm with a decreasing lithium concentration in the bulk is observed starting at 260 min (ca. 90 mAhr g^{-1}) into the potential hold, after which the rate of Li transport into the bulk increased considerably, propagating through the entire depth of Sn (12.5 μm) at 320 min (ca. 110 mAhr g^{-1}). The rate of Li incorporation into Sn at the near-surface region is equivalent to about 0.125 mA, while the actual electrochemical current is twice the amount at 0.2 mA (details of the data processing are described in the Supporting Information). This finding indicates parasitic losses of roughly 50% possibly towards solvent reduction, formation of the solid electrolyte interphase at the interface, and the reduction of naturally occurring surface SnO to Sn prior to Li transport into the material. Our observation (Figure 3) also points to a region

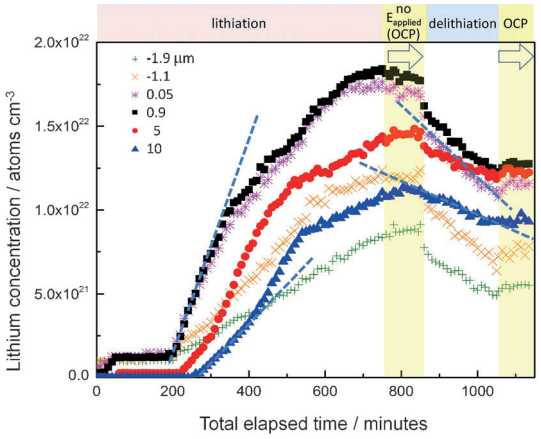

Figure 3. Lithium concentration at various regions of the battery as a function of lithiation (0 to 740 min) and removal of the applied potential (740–860 min), delithiation (860–1060 min), and removal of the applied potential (1060–1140 min).

between the near surface and the bulk (0.05 to 1 μm region) that shows faster rates of lithiation (i.e. steeper slopes, dashed lines in Figure 3) compared to lithiation of the bulk. From the observations of delithiation, it is also apparent that delithiation rates at the near-surface region occur much faster than the bulk (Figure 3).

The concentrations of lithium in pure Li_2Sn, LiSn, Li_7Sn_3, Li_5Sn_2, $Li_{13}Sn_5$, Li_7Sn_2, and $Li_{17}Sn_4$ are also plotted in Figure 2. It is evident that our material has not reached full lithiation, in part, to minimize electrode fracturing. Nevertheless, an expansion at the edge of the electrode/electrolyte (indicated by "*d*" between the vertical dashed lines in Figure 2) that is equivalent to an approximate 12% increase in thickness at 200 mAhr g^{-1} is observed. Most of the expansion seems to occur between 0 and 260 min, which arguably corresponds to literature reports on Li_2O formation.[2c]

The Li diffusion dynamics in the electrode can be modeled by Fick's law,[8] starting from the change in the concentration obtained from the NDP spectra and the flux of lithium from the electrochemical current. Two regions are apparent from our data (Figure 4 A), where a high diffusion coefficient of (ca. 1.5×10^{-7}–6×10^{-7} $cm^2 s^{-1}$) is observed during the initial charge and reaches relative consistent

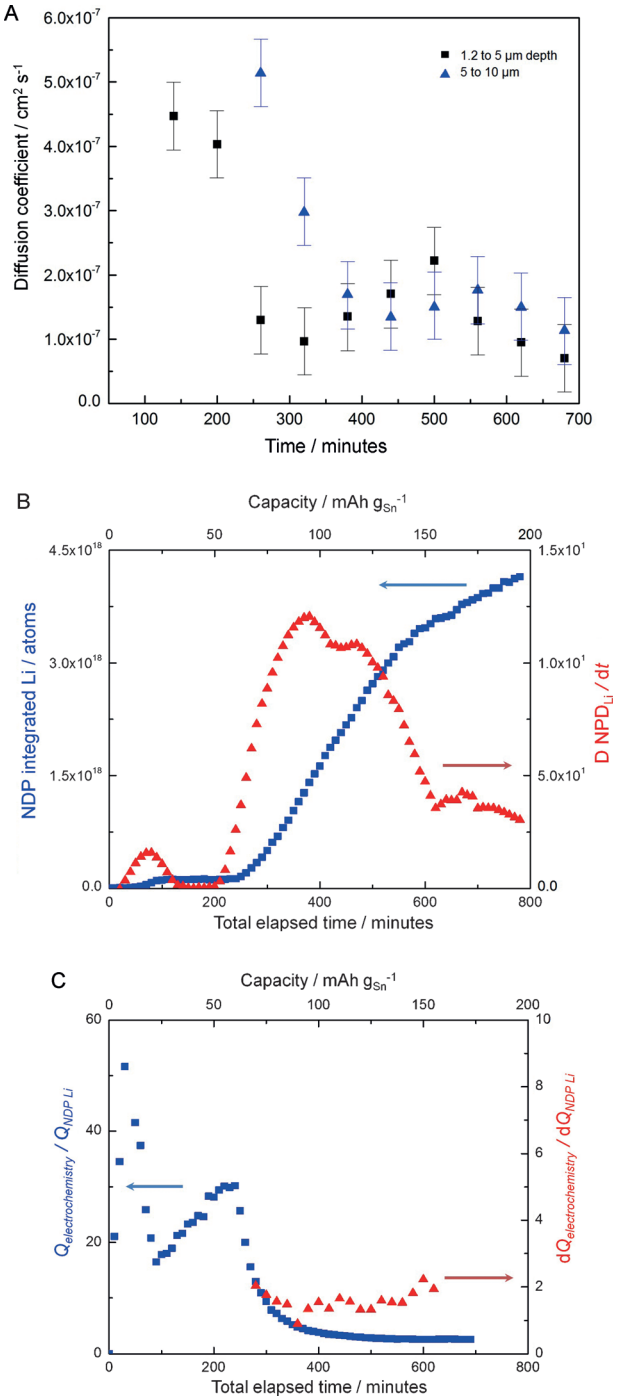

Figure 4. A) Li diffusion coefficient as a function of lithiation. B) Total integrated Li within the electrode (blue squares) and the change in Li concentration for every 10 min interval (red triangles). C) Ratio of electrochemical charge passed to the charge equivalent to the integrated Li (blue squares), and the ratio of the change in electrochemical charge passed and the corresponding change in the Li concentration for every 20 min interval (red triangles).

diffusion coefficient values of 0.7×10^{-7}–2.5×10^{-7} cm^2s^{-1} after 300 min. It was also observed that there is a delay in the lithiation deeper in the material (at 5–10 µm). A range of values have been reported for the diffusion constant of Li in Sn and other intermetallic compounds. The values obtained herein are in good agreement with literature values for Sn and Sn-based anodes at room temperature;[9] it is also comparable to Li diffusion coefficients in other Group IV elements,[10] Ge[11] and Si,[12] while values in the range of 10^{-12}–10^{-15} cm^2s^{-1} have also been suggested for some Sn-based alloys.[13] Noticeably, Li continues to diffuse into the material upon the removal of a lithiating potential (Figure 3), as evidenced by the decline in the near-surface Li concentration with time (from 740–860 min, when the electrode is at the open-circuit potential), while an increase in concentration is observed in the bulk of the electrode (at 5–10 µm in Figure 3). Clearly, Li continues to diffuse into areas of lower concentrations even after the applied potential is removed. Our previous studies on the in situ XRD analysis of a similar Sn film also corroborates this result, where Li_xSn is observed to rearrange three hours after the removal of an applied potential after lithiation. As expected, an overall decrease in the Li concentration is observed during delithiation (860–1060 min), with a higher delithiation rate occurring at the Sn/electrolyte interface and the near-surface region (0.05 and 0.9 µm) compared to the bulk (10 µm). Upon removal of the applied delithiation potential, the remaining Li concentration within the bulk remains unchanged (1060–1140 min).

The total amount of Li atoms present in the electrode was obtained by integrating the lithium concentration over the entire Sn film (0–13 µm). The change in Li atoms within the electrode for every 10 min interval was plotted against the total integrated Li over the lithiation period (Figure 4B). Our data show that while Li is detected on the electrode immediately during lithiation, significant amounts of Li incorporation into the material occurs between 200 and 500 min (ca. 50 to 100 $mAhr\,g^{-1}$), reaching a maximum increase at about 350 min (100 $mAhr\,g^{-1}$). It is apparent that the lithiation of Sn does not occur in uniform increments, despite the relatively constant current transient within the lithiation timeframe discussed. The amount of Li atoms detected by neutrons was converted into an "equivalent charge" which represents the charge consumed that resulted in a lithiated Sn electrode. A comparison between the electrochemical charge passed and the total Li atoms within the Sn film as a function of lithiation time is also plotted in Figure 4C.

A ratio of 1:1 between the electrochemical and Li NDP charge indicates that all of the electrochemical charge went into the conversion of Li_xSn, between 300 and 500 min (Figure 4C), whereas regions where the ratio is $>1:1$ implies that a portion of the measured electrochemical charge was consumed in "parasitic side reactions".[14] These parasitic reactions can be due to the electrochemical reduction of electrolyte species to form the solid electrolyte interphase (SEI) layer[15] and/or the reduction of native Sn surface oxides[16] to form a Li_2O matrix. Our results in Figure 4C indicate significant parasitic losses occurred during the first 230 min of charge. The rate of lithiation started to increase, as evidenced by the upward slope between 100 and 200 min and a downward slope between 230 and 320 min, while some electrochemical charge is still lost to parasitic reactions. After approximately 300 min, the ratio between the change in the electrochemical charge and the change in the NDP charge

appears to reach a plateau. This result indicates that a significant portion (70–100%) of the electrochemical charge was utilized for lithiation of the electrode material.

The experiment conducted also elucidates an interesting phenomenon occurring in the electrolyte region. Figure 2 shows an increase in the concentration of the electrolyte upon charging at relatively uniform increments with time. This increase in the Li concentration, which extends significantly into the electrolyte region (−5 to 0 μm) can be attributed to the concentration of the Li salt as a consequence of solvent consumption during the formation of the SEI or due to a decrease in the volume from the expansion of the electrodes. Another possible reason for this observation is the preferential migration of ^{6}Li towards Sn during lithiation,[17] which induces an enrichment of ^{6}Li at the surface.

The experiments presented here illustrate the capability of in situ NDP to probe Li transport and distribution across the electrode interface and in the electrode in real time. This method can be used to investigate an extensive range of anodes and cathodes, not limited to intermetallic-forming materials. The in situ NDP technique is a very promising diagnostic tool for the development of a comprehensive range of materials as architectures for specific purposes (high energy versus high power applications). For example, this method can resolve some of the issues concerning the Li trapped within localized pockets in the electrode that result in low coulombic efficiencies; provide understanding of requirements for optimum materials architecture that promote efficient Li transport, which is often the rate-limiting phenomenon in battery processes; gain insight in materials properties for high rates of Li transport; and provide a direct experimental verification method for models predicting mass and charge transfer in Li-ion cells, including failure and aging mechanisms.

We have shown in situ NDP to be an invaluable technique that complements other methods for the characterization of materials that are necessary to contribute to our comprehension of the complex interrelation between electrochemistry, kinetics of Li reactions, intercalation, and transport. This understanding is indispensable for the development of reactions and morphologies that will enable the advancement of materials for energy storage.

Received: April 10, 2014
Published online: July 14, 2014

Keywords: analytical chemistry · electrochemistry · lithium-ion batteries · neutron depth profiling · tin

[1] a) K. Persson, V. A. Sethuraman, L. J. Hardwick, Y. Hinuma, Y. S. Meng, A. van der Ven, V. Srinivasan, R. Kostecki, G. Ceder, *J. Phys. Chem. Lett.* **2010**, *1*, 1176–1180; b) B. Scrosati, *J. Electrochem. Soc.* **1992**, *139*, 2776–2781.

[2] a) F. Blanc, M. Leskes, C. P. Grey, *Acc. Chem. Res.* **2013**, *46*, 1952–1963; b) J. Y. Huang, L. Zhong, C. M. Wang, J. P. Sullivan, W. Xu, L. Q. Zhang, S. X. Mao, N. S. Hudak, X. H. Liu, A. Subramanian, H. Fan, L. Qi, A. Kushima, J. Li, *Science* **2010**, *330*, 1515–1520; c) M. Ebner, F. Marone, M. Stampanoni, V. Wood, *Science* **2013**, *342*, 716–720; d) D. E. Conte, M. Mouyane, L. Stievano, B. Fraisse, M. T. Sougrati, J. Olivier-Fourcade, P. Willmann, C. Jordy, M. Artus, S. Cassaignon, K. Driezen, J.-C. Jumas, *J. Solid State Electrochem.* **2012**, *16*, 3837–3848; e) Y. Tian, A. Timmons, J. R. Dahn, *J. Electrochem. Soc.* **2009**, *156*, A187–A191.

[3] a) S. Whitney, S. R. Biegalski, Y. H. Huang, J. B. Goodenough, *J. Electrochem. Soc.* **2009**, *156*, A886–A890; b) R. G. Downing, G. P. Lamaze, J. K. Langland, S. T. Hwang, *J. Res. Natl. Inst. Stand. Technol.* **1993**, *98*, 109–126.

[4] C.-M. Park, J.-H. Kim, H. Kim, H.-J. Sohn, *Chem. Soc. Rev.* **2010**, *39*, 3115–3141.

[5] P. Limthongkul, Y. I. Jang, N. J. Dudney, Y. M. Chiang, *Acta Mater.* **2003**, *51*, 1103–1113.

[6] a) J. Zhu, C. Gladden, N. Liu, Y. Cui, X. Zhang, *Phys. Chem. Chem. Phys.* **2013**, *15*, 440–443; b) Z. Wei Seh, W. Li, J. J. Cha, G. Zheng, Y. Yang, M. T. McDowell, P.-C. Hsu, Y. Cui, *Nat. Commun.* **2013**, *4*, 1331–1331; c) A. G. Dylla, G. Henkelman, K. J. Stevenson, *Acc. Chem. Res.* **2013**, *46*, 1104–1112.

[7] J. F. M. Oudenhoven, F. Labohm, M. Mulder, R. A. H. Niessen, F. M. Mulder, P. H. L. Notten, *Adv. Mater.* **2011**, *23*, 4103.

[8] R. A. Flinn, P. K. Trojan, *Engineering materials and their applications*, Houghton Mifflin, Boston USA, **1986**.

[9] a) C. J. Wen, R. A. Huggins, *J. Solid State Chem.* **1980**, *35*, 376–384; b) M. Winter, J. O. Besenhard, *Electrochim. Acta* **1999**, *45*, 31–50.

[10] C. S. Fuller, J. C. Severiens, *Phys. Rev.* **1954**, *96*, 21–24.

[11] J. Graetz, C. C. Ahn, R. Yazami, B. Fultz, *J. Electrochem. Soc.* **2004**, *151*, A698–A702.

[12] C.-Y. Chou, G. S. Hwang, *Surf. Sci.* **2013**, *612*, 16–23.

[13] a) J. Xie, N. Imanishi, A. Hirano, Y. Takeda, O. Yamamoto, X. B. Zhao, G. S. Cao, *Solid State Ionics* **2010**, *181*, 1611–1615; b) J. O. Besenhard, M. Wachtler, M. Winter, R. Andreaus, I. Rom, W. Sitte, *J. Power Sources* **1999**, *81–82*, 268–272.

[14] Y. Matsumura, S. Wang, J. Mondori, *J. Electrochem. Soc.* **1995**, *142*, 2914–2918.

[15] E. Peled, *J. Electrochem. Soc.* **1979**, *126*, 2047–2051.

[16] a) S. D. Beattie, T. Hatchard, A. Bonakdarpour, K. C. Hewitt, J. R. Dahn, *J. Electrochem. Soc.* **2003**, *150*, A701–A705; b) W. E. Boggs, R. H. Kachik, G. E. Pellissier, *J. Electrochem. Soc.* **1961**, *108*, 6–12; c) W. E. Boggs, P. S. Trozzo, G. E. Pelissier, *J. Electrochem. Soc.* **1961**, *108*, 13–24; d) W. E. Boggs, *J. Electrochem. Soc.* **1961**, *108*, 124–129.

[17] S. Yanase, T. Oi, S. Hashikawa, *J. Nucl. Sci. Technol.* **2000**, *37*, 919–923.

